Ultrasonics Sonochemistry 121 (2025) 107519

Contents lists available at ScienceDirect

Ultrasonics Sonochemistry

journal homepage: www.elsevier.com/locate/ultson

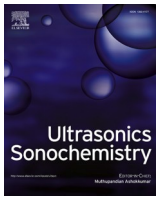

Sonochemical oxidation activity in 20-kHz probe systems: The effects of vessel shape, vessel wall thickness, and probe position☆

Chaewoon Hwang [1], Iseul Na [1], Younggyu Son [*]

Department of Environmental Engineering, Kumoh National Institute of Technology, Gumi 39177, Republic of Korea

ARTICLE INFO

Keywords:
Geometric optimization
Probe position
Vessel shape
Vessel wall thickness
KI dosimetry
BPA degradation

ABSTRACT

As a follow-up to our previous studies aimed at optimizing the use of the 20 kHz probe system in chemical and environmental engineering processes, the effects of vessel shape, vessel wall thickness, and probe position on sonochemical oxidation activity in circular and rectangular acrylic vessels were investigated. Electrical and calorimetric powers were obtained, and the sonochemical oxidation activity was quantified using KI dosimetry (pseudo-zero-order reaction kinetics) under 42 geometric conditions. All the geometric conditions of vessel shape, wall thickness, and probe position significantly affected the magnitudes and trends of the sonochemical activity. The average power conversion efficiencies from electrical to calorimetric power were 47.9 ± 3.0 % and 50.3 ± 6.1 % for circular and rectangular vessels, respectively. Overall, much higher activity was obtained when the probe was placed close to the bottom of the circular and rectangular vessels. Average volume-modified zero-order reaction rate constants were 0.20 ± 0.09 and 0.29 ± 0.08 μmol/min for the circular vessels with wall thicknesses of 5 and 10 mm and rectangular vessels with wall thicknesses of 5, 10, 15, and 20 mm. However, the probe positions for the highest activity moved toward to the liquid surface as the thickness increased in the rectangular vessels. The variation in the sonochemical activity was well visualized in the sonochemiluminescence (SCL) image (side and bottom views) analysis, and a higher intensity was observed in the SCL images when the probe was positioned adjacent to the vessel bottom. Thus, the total intensities of the SCL matched well with those of the sonochemical activity using KI dosimetry. Significantly different trends were observed in the BPA degradation tests, which may be attributed to the difference between the zero-order and first-order reactions.

1. Introduction

Acoustic cavitation has been widely investigated for the development of innovative advanced oxidation–reduction processes (AORPs) with other novel technologies, including UV, ozone, catalysts, and oxidizing agents, for the eco-friendly removal of emerging micropollutants in the chemical and environmental engineering fields [1–10]. Recently, it has also been reported that per- and polyfluoroalkyl substances (PFAS), also known as forever chemicals, can be effectively removed in sonochemical processes [11–13].

The effectiveness of cavitational removal of aqueous pollutants is primarily affected by the ultrasonic conditions, including frequency and power, solution conditions, including temperature, dissolved gases, and pH, and target contaminant conditions, including volatility/solubility and initial concentration [14,15]. Several research groups have reported that geometric optimization, including that of the reactor shape, size, transducer position, liquid height/volume, and mixing/sparging in sonoreactors, can significantly enhance sonochemical and sonophysical effects under similar input power conditions [16–32]. Slight changes in the geometric conditions can result in significant changes in the formation of cavitational active zones, leading to remarkable differences in the cavitational activity [26]. Recently, AI techniques such as machine learning have been used to predict removal efficiencies and reaction kinetic constants using accumulated research results in the fields of sonochemistry and environmental engineering fields [33–35]. However, more research data regarding geometric conditions are required to make more accurate predictions using AI techniques.

We have investigated various geometric effects in 20 kHz probe systems, one of the most commonly used ultrasonic devices in laboratories, as basic steps for understanding and designing various

☆ This article is part of a special issue entitled: 'Cavitation Bubbles and Sonochemical Activity' published in Ultrasonics Sonochemistry.

* Corresponding author.
E-mail address: yson@kumoh.ac.kr (Y. Son).

[1] The authors equally contributed to this study as first authors.

https://doi.org/10.1016/j.ultsonch.2025.107519
Received 1 July 2025; Received in revised form 29 July 2025; Accepted 16 August 2025
Available online 23 August 2025

cavitational applications: 1) The effects of the probe positions, input power, liquid height/volume, and bottom thickness on sonochemical oxidation reactions were investigated in glass vessels (100, 250, 500, and 1,000 mL), and it was found that the probe positions predominantly affected the degree of sonochemical reactions [23,36]. 2) Relatively large vessels [0.18 L (D = 5 cm), 0.90 L (D = 10 cm), 3.60 L (D = 20 cm), and 8.40 L (D = 30 cm)] were tested for the 20 kHz probe systems to evaluate the applicable maximum sizes and the highest sonochemical oxidation activities based on the mass of the products were obtained in the vessel with the diameter of 20 cm with the strongest sonochemiluminescence (SCL) intensity [16]. 3) The degassing effect was investigated in a 500 mL glass vessel, and it was found that the degassing behavior varied depending on the probe position [20]. In addition, a significant reduction in dissolved oxygen concentration was observed even under continuous O_2 and Ar/O_2 mixture sparging conditions. 4) Ultrasonic desorption was investigated using paint-coated glass beads in 500 mL glass vessels, and it was found that the degree of ultrasonic desorption was also significantly affected by the probe positions [37].

In this study, the effects of probe position, vessel shape, and wall thickness on sonochemical oxidation activity were investigated in six different acrylic vessels equipped with a 20 kHz probe as a follow-up to our previous studies [16,20,23,36,37] to suggest guidelines for the appropriate use of 20 kHz probe systems and accumulate experimental results for the AI database. Electrical and calorimetric powers were obtained under various geometric conditions, and the sonochemical oxidation activity was quantified using KI dosimetry. SCL images for all cases were captured from the side and bottom views to visualize the sonochemically active zone. In addition, BPA degradation was investigated under various geometric conditions.

2. Materials and methods

2.1. Chemicals

Potassium iodide (KI) and sodium hydroxide (NaOH) were obtained from Junsei Chemical Co., Ltd. (Tokyo, Japan). An iodine (I_2) solution (0.05 M) was acquired from Merck (Darmstadt, Germany). Luminol (3-aminophthalhydrazide, $C_8H_7N_3O_2$) and BPA ($C_{15}H_{16}O_2$) were purchased from Sigma–Aldrich (St. Louis, MO, USA). All chemicals were used as received.

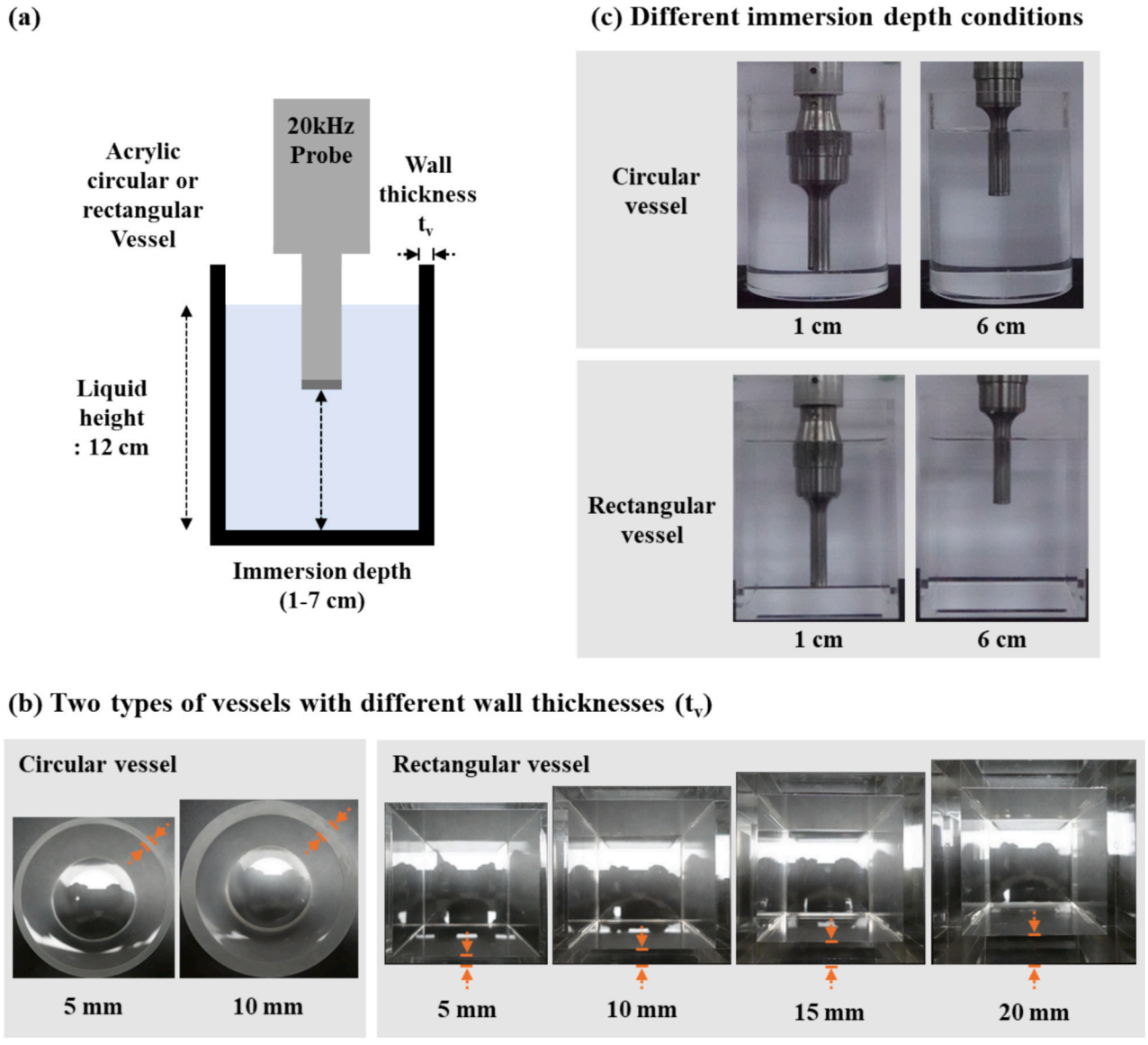

Fig. 1. (a) Schematic of the experimental setup (t_v: vessel wall thickness); (b) Circular and rectangular vessels with different wall thicknesses; (c) Different immersion depths.

2.2. Experimental setup

Fig. 1 shows a schematic of the experimental setup used in this study. A 20-kHz horn-type (or probe-type) sonicator (VCX–750, Sonics & Materials Inc., USA), equipped with a threaded-end type probe and a replaceable tip of 13 mm diameter, made of a titanium alloy, was used in this study. Six geometrically different vessels, including two acrylic circular vessels (inner diameter: 10 cm; height: 15 cm; wall thicknesses: 5 and 10 mm) and four acrylic rectangular vessels (length: 10 cm; width: 10 cm; height: 15 cm; wall thicknesses: 5, 10, 15, and 20 mm), were used, and the probe was submerged in the vessels. In this study, the walls include the bottom and cylindrical walls in the circular vessels, and the bottom and four sidewalls in the rectangular vessels. To maintain the liquid height in the vessels at 12 cm for all cases under different probe submerging depths, the liquid volume varied from 0.88 to 0.92 L and from 1.14 to 1.19 L for circular and rectangular vessels, respectively.

The temperature of the liquid body was maintained at 25 ± 2 °C. The probe immersion depth and distance from the probe tip end to the bottom surface of the vessel varied from 1 cm to 7 cm [16,23]. The input power of the probe was 50 %, which was considered to be the power level of the device. The electrical energy consumption of the sonicator, referred to as electrical power (P_{elec}) in this study, was measured using a power meter (HPM-300A, ADpower, KOR) equipped with a data logger. The ultrasonic energy, termed calorimetric power (P_{cal}) in this study, was calculated using the following equation:

$$P_{cal} = \frac{dT}{dt} C_P M \quad (1)$$

where P_{cal} is the ultrasonic/calorimetric energy; dT/dt is the rate of increase of the liquid temperature; C_p is the specific heat capacity of the liquid (4.184 J/(g·K) for water); and M is the mass of the liquid [16,18,23].

2.3. Quantification of sonochemical oxidation activity

The sonochemical oxidation reactions were quantified using KI dosimetry and BPA degradation for zero- and first-order reaction analyses, respectively [9,18]. The initial concentrations of the KI solution and BPA were 1 g/L (6.02 mM) and 5 mg/L (0.022 mM), respectively, and the irradiation times were 10 min and 60 min, respectively. To conduct the KI dosimetry and BPA degradation experiments under the same geometric conditions, no additional cooling system was applied. The 10-min ultrasound irradiation followed by ice cooling was repeated for 60 min to maintain the temperature in the liquid for the BPA degradation experiments. The final sonochemical product, triiodide (I_3^-), was detected using a UV–Vis spectrophotometer (Libra S60; Biochrom Ltd., UK), while the BPA was detected using an HPLC system (1260 Infinity II LC, Agilent, USA) [18]. To analyze the sonochemical oxidation activity under different input power conditions (P_{elec} and P_{cal}), the input power-normalized reaction kinetic constants were compared.

2.4. Visualization of sonochemical oxidation reactions

The sonochemically active zone was visualized using a luminol solution (0.1 g/L luminol and 1 g/L NaOH) in a completely dark room [19,23,36,37]. Sonochemiluminescence (SCL) images were captured using an exposure-controlled digital camera (-RX100 VII; Sony Corp., Japan). The exposure time was set to 10 s. The SCL images were analyzed using ImageJ software to obtain the SCL intensity [23,38,39].

3. Results and discussion

3.1. Calorimetric power and KI dosimetry

The sonochemical oxidation activity was quantitatively investigated using KI dosimetry in the 20 kHz probe systems under various geometric conditions, including reactor shapes (circular and rectangular), probe positions (1, 2, 3, 4, 5, 6, and 7 cm from the bottom), and wall thicknesses (5, 10, 15, and 20 cm). Fig. 2 shows the measured electrical power (P_{elec}) and calorimetric power (P_{cal}) under all the applied conditions. The electrical and calorimetric powers varied significantly from 98.0 to 145.1 W and from 45.3 to 79.3 W, respectively, depending on the geometric conditions applied. Higher electrical and calorimetric powers were obtained when the probe was positioned adjacent to the bottom of the vessel. Son et al. reported that the electrical and calorimetric powers remained constant and then increased as the probe approached the bottom of the glass vessel in the 20 kHz probe systems [23]. In this study, similar trends in the electrical and calorimetric powers were observed for the circular vessels with wall thicknesses of 5 and 10 mm and rectangular vessel with a wall thickness of 5 mm, as shown in Fig. 2 (a)–(c). However, significantly different trends were observed for the rectangular vessel cases with wall thicknesses of 10, 15, and 20 mm, as shown in Fig. 2(d)–(f), where it is observed that the electrical power increased relatively linearly and the calorimetric power increased relatively nonlinearly as the probe approached the bottom.

Overall, the calorimetric power increased with the electrical power (No significant linear relationship was not observed in this study.) [23]. The average power conversion efficiency from electrical to calorimetric power was 49.6 ± 5.5 % for all cases (circular vessels: 47.9 ± 3.0 %; rectangular vessels: 50.3 ± 6.1 %). It should be noted that significantly different calorimetric powers were obtained under similar electric powers or vice versa for some cases: the calorimetric powers were 51.0 W and 74.6 W for the circular vessel with t_v = 5 mm and probe position = 2 cm (P_{elec}: 120.7 W) and the rectangular vessel with t_v = 20 mm and probe position = 3 cm (P_{elec}: 120.2 W), respectively; the electrical powers were 127.6 W and 99.9 W for the rectangular vessel with t_v = 5 mm and probe position = 2 cm (P_{cal}: 52.6 W) and the rectangular vessel with t_v = 15 mm and probe position = 7 cm (P_{elec}: 52.6 W), respectively. It was reported that the variations in the calorimetric powers under similar electrical powers, and vice versa, were attributed to the differences in the impedance of the ultrasonic transducer resulting from different geometric conditions [16,40,41]. As the electrical impedance of the piezoelectric transducer decreases, the transducer can vibrate more easily and generate ultrasonic power with a higher amplitude [42].

It has been reported that a slight change in liquid height can result in a significant difference in sonochemical activity [25–28,43–45]. Thus, volume-modified zero-order reaction rate constants were obtained using the following equation because the liquid height in the vessels was fixed at 12 cm in this study and the liquid volume slightly decreased as the probe immersion depth increased [circular reactor: 7 cm (0.92 L) → 1 cm (0.89 L); rectangular reactor: 7 cm (1.19 L) → 1 cm (1.14 L)]:

$$\frac{dm}{dt} = V\frac{dC}{dt} = Vk_0 = k_0' \quad (2)$$

where m is the mass of the sonochemical product (I_3^- ions), V is the liquid volume in the vessel, C is the concentration of the sonochemical product (I_3^- ions), k_0 is the pseudo-zero-order reaction kinetic constant, and k_0' is the volume-normalized pseudo-zero-order reaction kinetic constant.

For wall thicknesses of 5 and 10 mm in the circular and rectangular vessels, relatively higher sonochemical activities (k_0') were observed at probe positions of 1 and 2 cm, as shown in Fig. 2(a)–(d). It should be noted that the magnitudes of sonochemical activity at 1 and 2 cm were significantly different. It has been reported that a stronger ultrasound reflection occurs without significant attenuation as the probe approaches the vessel bottom [16,23]. This could lead to the expansion of the cavitational active zone with a strong intensity and enhancement of the sonochemical oxidation activity. For all probe positions, similar trends in sonochemical activity were observed for the circular vessels with thicknesses of 5 and 10 mm, and the rectangular vessel with a thickness of 5 mm. However, different trends were observed for the

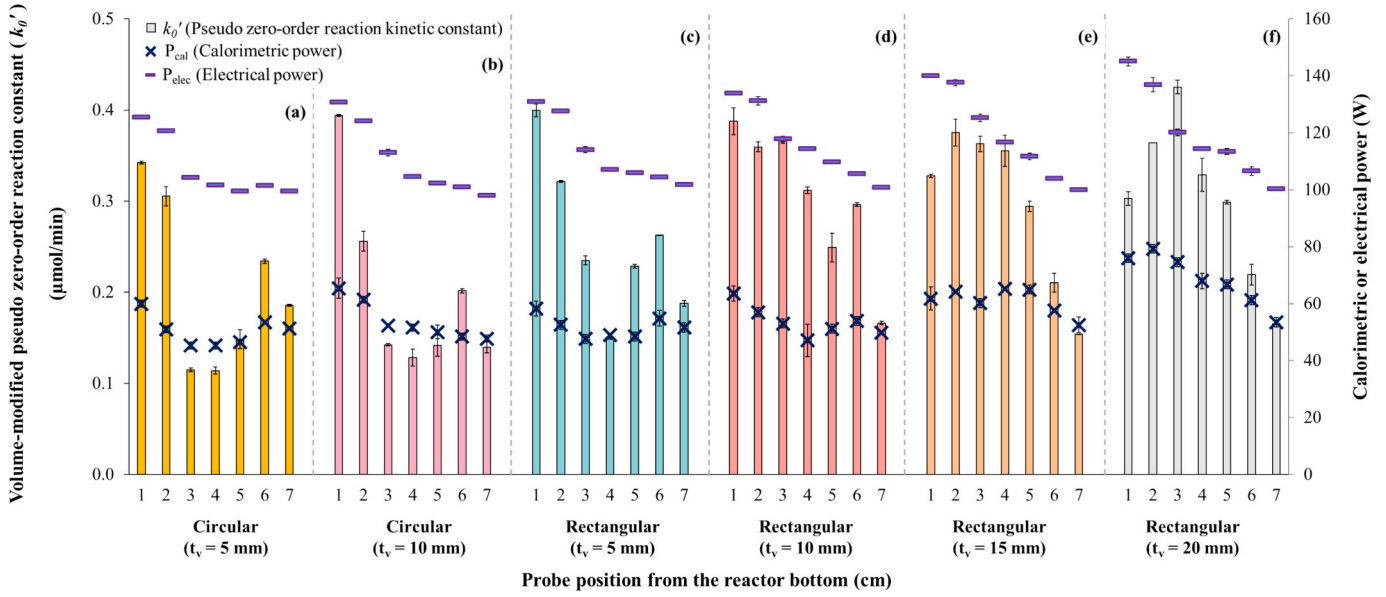

Fig. 2. Volume-modified pseudo zero-order reaction constants (k_0'), calorimetric powers, and electrical powers under various geometric conditions (all the data points include error bars).

rectangular vessels with thicknesses of 5, 10, 15, and 20 mm, as shown in Fig. 2(c)–(f), where relatively high activities were obtained at probe positions of 1–5 cm in comparison to those at 1–5 cm in Fig. 2(a)–(c). In addition, the probe position for the highest activity moved further from the vessel bottom as the wall thickness increased. The highest activities were obtained at 2 and 3 cm, and the increases in the highest activities were 14.5 % and 40.3 % compared with those at 1 cm for wall thicknesses of 15 and 20 mm, respectively.

There were no significant differences in the ultrasound reflection coefficients (R) obtained using the following equations in the simplified three-layered system (water/acrylic wall/air) for wall thicknesses of 5–100 mm, as shown in Fig. 1S:

$$R = R_{12} + \frac{T_{12}\,T_{21}\,R_{23}\,e^{2ik_2d}}{1 - R_{21}\,R_{23}\,e^{2ik_2d}} \tag{3}$$

$$R_{12} = \frac{z_2 - z_1}{z_2 + z_1} \tag{4}$$

$$R_{23} = \frac{z_3 - z_2}{z_3 + z_2} \tag{5}$$

$$T_{12} = \frac{2z_2}{z_2 + z_1} \tag{6}$$

where R_{12} and T_{12} are the pressure reflection and transmission coefficients at the water/acrylic wall interface, respectively; R_{21} and T_{21} are the pressure reflection and transmission coefficients at the acrylic wall/water interface; R_{23} is the pressure reflection coefficient at the acrylic wall/air interface; k_2 is the wavenumber in the acrylic wall; d is the thickness of the acrylic wall; and z_1, z_2, and z_3 are the acoustic impedances of water, acrylic wall, and air, respectively [46,47]. The reflection coefficients ranged from 0.9990 to 0.9997, indicating that almost 100 % ultrasound reflection occurred for wall thicknesses in the range of 5–100 mm in the simplified system. However, a large difference in sonochemical activity was observed for various wall thicknesses in this study. It has been reported that the simulated acoustic pressure distributions in 20 kHz probe systems do not correspond to the spatial distributions of sonochemical oxidation activity (SCL images) [23,48,49].

As shown in Fig. 2S, as the electrical or calorimetric power increases, the volume-modified zero-order reaction rate constant (k_0') also increases. However, the relationships were not strongly linear: the calorimetric power increased by 32.5 % (45.3 W → 60.0 W) and the k_0' value increased by 168.4 % (0.014 → 0.306 μmol/min) when the probe moved from 3 cm to 1 cm in the circular vessel with the thickness of 5 mm; the calorimetric powers were similar (53.9 and 53.0 W) and the k_0' value increased by 23.7 % (0.296 → 0.366 μmol/min) when the probe moved from 6 cm to 3 cm in the rectangular vessel with the thickness of 10 mm; the highest k_0' value was obtained at the third highest calorimetric power condition in the rectangular vessel with the thickness of 20 mm. Therefore, the comparison of volume-modified pseudo-zero-order reaction constants (k_0') under various geometric conditions may be inappropriate from a scientific and engineering perspective because the constants were obtained under different electrical and calorimetric power conditions. From a scientific perspective, the mechanisms of sonochemical reactions can be understood using calorimetric power, and from an engineering perspective, sonochemical reactions can be analyzed economically using electrical power [25,26,50]. Thus, energy- and volume-modified pseudo-zero-order reaction constants (k_0''), which represent the mass of sonochemical products (I_3^- ions) per unit time and unit power and correspond to the cavitation yield in previous studies [25,26,28,43], were calculated using the following equation:

$$k_0'' = \frac{k_0'}{P_{cal}} \text{ or } \frac{k_0'}{P_{elec}} \tag{7}$$

As shown in Fig. 3, the relative magnitudes and overall trends of the energy- and volume-modified pseudo-zero-order reaction constants (k_0'') were similar to those of the volume-modified pseudo-zero-order reaction constants (k_0') because of the small difference in the electrical and calorimetric powers. For the calorimetric-power-related k_0'' (k_0' / P_{cal}), the average value of k_0'' for all conditions was 0.0045 ± 0.0025 μmol/W/min. Moreover, the average values were 0.0038 ± 0.0013 and 0.0049 ± 0.0012 μmol/W/min for the circular and rectangular vessels, respectively. This indicated that more sonochemical reactions could occur under the same calorimetric power conditions. For the electrical-power-related k_0'' (k_0' / P_{elec}), the average value of k_0'' for all conditions was 0.0022 ± 0.0006 μmol/W/min. In addition, the average values were 0.0018 ± 0.0006 and 0.0024 ± 0.0005 μmol/W/min for the circular and rectangular vessels, respectively. This indicates that rectangular vessels are more advantageous in terms of energy efficiency.

It was found that the probe positions for the highest activity in terms

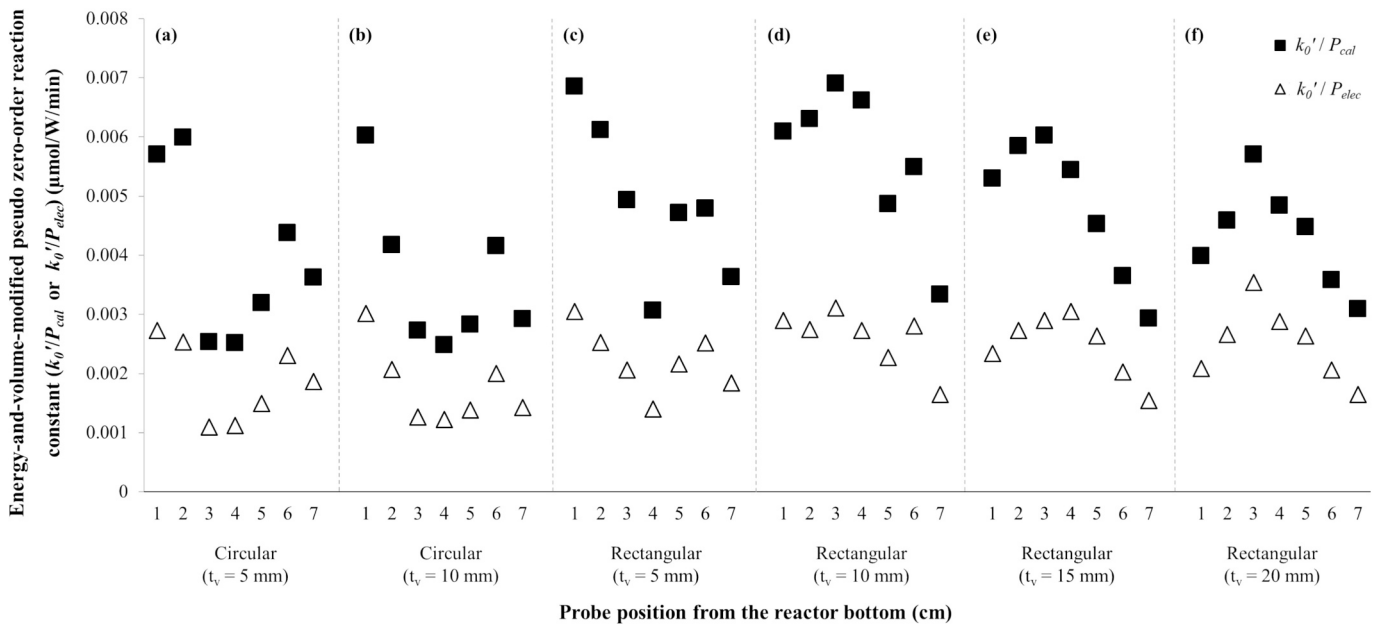

Fig. 3. Energy-volume-modified pseudo zero-order reaction constants using the electrical and calorimetric powers under various geometric conditions.

of k_0'' changed in rectangular vessels with thicknesses of 10 and 15 mm compared to those in terms of k_0' [the probe positions for the highest k_0': 1 cm for 5 mm t_v; 1 cm for 10 mm t_v; 2 cm for 15 mm t_v; 3 cm for 20 mm t_v; the probe positions for the highest k_0'': 1 cm for 5 mm t_v; 3 cm for 10 mm t_v; 3 cm (P_{cal}) and 4 cm (P_{elec}) for 15 mm t_v; 3 cm for 20 mm t_v]. In addition, the highest calorimetric-power-related k_0'' (k_0' / P_{cal}) values for each thickness condition decreased significantly, as the wall thickness increased because higher calorimetric powers were obtained in the rectangular vessel with the thicker wall (the average calorimetric power depending on the wall thickness: 5 mm: 52.8 W ± 5.3 W; 10 mm: 57.9 W ± 5.3 W; 15 mm: 62.1 W ± 2.0 W; 20 mm: 76.6 W ± 2.4 W). The significant difference in the calorimetric power may be due to the difference in heat loss from the liquid phase to the vessel wall, depending on the wall thickness, when the temperature increases in the liquid phase by ultrasound irradiation [25]. Toma et al. reported that the consumed electrical energy was converted into ultrasonic energy, heat energy in the transducer, liquid atomization energy, and energy lost to the surrounding environment [51]. No significant decrease in the highest electrical-power-related k_0'' (k_0' / P_{elec}) values was observed. Thus, the optimal geometric conditions for sonochemical activity per unit time and power can vary depending on the electrical or calorimetric power.

3.2. SCL image analysis

As mentioned above, the relationship between the electrical power and calorimetric power and that between the calorimetric power and volume-modified pseudo-zero-order reaction constants (k_0') were not highly linear. This may be attributed to the complicated characteristics of the sound pressure distribution and sonochemical active zone formation under different geometric conditions. As shown in Fig. 4, SCL images from the side and bottom views were obtained to visually investigate the formation of the sonochemically active zone under all the applied geometric conditions in this study. Bottom-view images, taken to overcome the limitations of two-dimensional images, enable a better understanding of the shape, dimensions, and symmetry of the sonochemically active zone in three dimensions [16,21,23].

SCL images with diverse patterns were obtained depending on the vessel shape, probe position, and vessel wall thickness. The active zone (bright area) was divided into three regions: 1) region under the probe tip, 2) the bottom region, and 3) the region surrounding the immersed probe body [23]. As the probe approached the bottom of the vessel, brighter light was observed over a wide area in the region under the probe tip and surrounding the probe. Consequently, stronger and larger sonochemically active zones formed in the three regions, and higher sonochemical activity was obtained when the probe was placed adjacent to the bottom, as shown in Fig. 2 [16,20,23,36]. As mentioned above, this was attributed to the strong reflection of the ultrasound at the bottom of the vessel. As the probe moved up to the liquid surface, the effects of the vessel shape and wall thickness seemed to be less significant.

In the bottom-view SCL images of the circular vessels, concentric circles were observed around the center of the vessel, and they were considered to be the formation of a standing wave field owing to the uniform distance from the center to the sidewall [16,26]. Larger, thicker, and more distinct cylindrical zones were observed when the probe was placed at the bottom. In addition, very similar SCL images were observed at each probe position in the circular vessels with thicknesses of 5 and 10 mm, resulting in no significant difference in the sonochemical activity, as shown in Fig. 2.

In the SCL images of the rectangular vessels, a more active zone was formed, leading to enhanced sonochemical activities and higher average values of the reaction constants when the probe was placed at mid-height positions (3–5 cm), compared to those of the circular vessels. Similar active zones, consisting mainly of regions 1) and 2), were formed when the probe was positioned closer to the liquid surface. However, a bright light was detected at the four centers when the probe approached the bottom. This could be due to the various distances from the center to the side wall and the more complicated ultrasound reflection and transmission. Yang et al. simulated the acoustic pressure fields in a rectangular bath-type sonoreactor equipped with a single 40 kHz transducer at the center of the reactor bottom and reported that high-pressure regions formed at the center and four corners, especially in smaller sonoreactors [52]. Depending on the wall thickness, the SCL pattern variation was divided into three categories: 1) 5 mm, 2) 10 mm, and 3) 15 and 20 mm. In addition, the active zone expanded toward the sidewall as the wall thickness increased. Yasui et al. (2007) reported that thicker sonoreactor walls provide more stable boundary conditions for ultrasound irradiation [53]. Consequently, these differences may induce distinctly different trends in the pseudo-reaction constants shown in

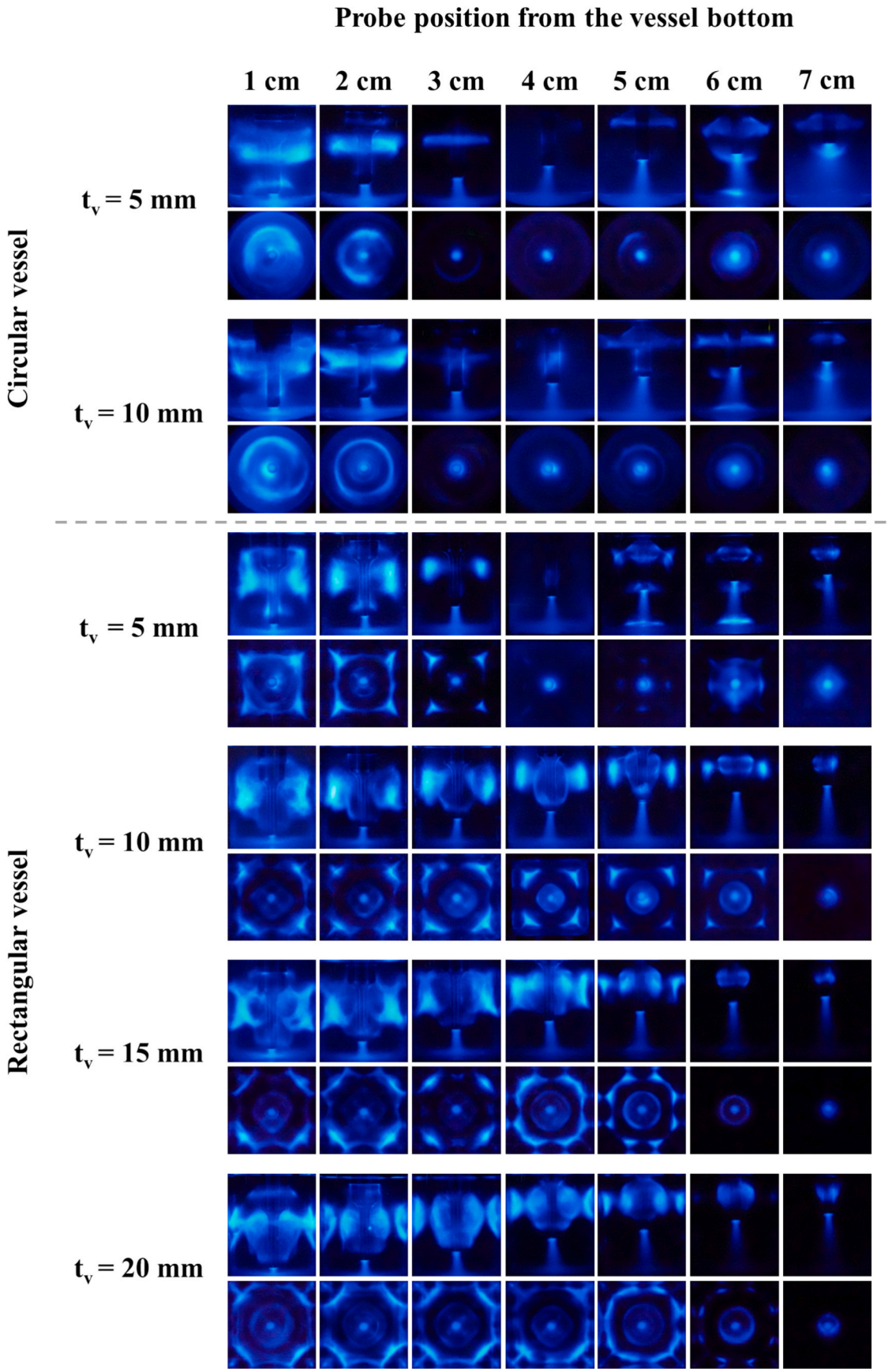

Fig. 4. SCL images from side and bottom view under various geometric conditions. Images from the first and second layers at each thickness condition were captured from the side and bottom views, respectively.

Figs. 2 and 3.

To investigate the correlation between the SCL intensity and the volume-modified pseudo-zero-order reaction constant (k'_0), the SCL intensities were quantified using image analysis software and compared with the reaction constants, as shown in Fig. 3S [23,38,39,54]. Although the SCL images could provide a cross-sectional interpretation of the three-dimensional active zone, the trends of the SCL intensities of both the side and bottom views relatively matched with those of the constants [16,23]. This may be because the KI dosimetry and SCL methods are based on cavitation-induced radical oxidation reactions. It should be noted that distortion of the SCL images and a decrease in SCL intensity could occur as the wall thickness increases. Capturing SCL images from more viewpoints and creating three-dimensional structures will allow for a better understanding of the formation and optimization of the sonochemically active zone and better correlation with target sonochemical reactions [16].

3.3. BPA degradation

The effect of wall thickness on BPA degradation was investigated in rectangular vessels with thicknesses of 5, 10, 15, and 20 mm, as shown in Fig. 5. The probe was positioned 1, 2, and 3 cm from the bottom, where a higher sonochemical activity (KI dosimetry) was obtained. The sonochemical degradation of BPA followed pseudo-first-order kinetics. Because the liquid volume changed by a maximum of only 1.72 % with applied probe positions [3 cm (1.16 L) → 1 cm (1.14 L)], the pseudo-first-order reaction constants (k_1) were not modified using the applied volume [9,18]. The pseudo-first-order reaction constants remained relatively constant under each thickness condition, except for the case of 5 mm, and these trends were different from those of the volume-modified pseudo-zero-order reaction constants (k'_0). In addition, the average constant for the probe positions of 1, 2, and 3 cm decreased (5 mm: 0.0062 ± 0.0008 min^{-1}; 10 mm: 0.0054 ± 0.0002 min^{-1}; 15 mm: 0.0044 ± 0.0002 min^{-1}; 20 mm: 0.0048 ± 0.0001 min^{-1}) as the thickness increased. The pseudo-zero-order reaction constants for the probe positions of 1, 2, and 3 cm in the KI dosimetry tests were 0.32 ± 0.08 μmol/min, 0.37 ± 0.01 μmol/min, 0.36 ± 0.02 μmol/min, and 0.36 ± 0.06 μmol/min for the thickness of 5, 10, 15, and 20 mm, respectively. These differences might be due to the difference between zero-order reactions, where the reactant concentration was maintained, and first-order reactions, where the reactant concentration decreased over time. Lee and Son reported that sonochemical reactions for removals of aqueous pollutants generally followed first-order reaction kinetics and direct comparisons between zero- and first-order reactions are difficult [18]. Thus, the optimal conditions under various geometric conditions can vary significantly depending on the characteristics of the target reactions.

In addition, the average calorimetric and electrical power increased as the thickness increased (5 mm: P_{cal} = 52.4 ± 3.1 W, P_{elec} = 124.2 ± 8.9 W; 10 mm: P_{cal} = 55.6 ± 2.2 W, P_{elec} = 127.7 ± 8.6 W; 15 mm: P_{cal} = 59.9 ± 6.0 W, P_{elec} = 134.3 ± 7.9 W; 20 mm: P_{cal} = 64.4 ± 5.0 W, P_{elec} = 134.0 ± 12.7 W). Accordingly, the energy-modified pseudo-zero-order reaction constants obtained using Eq. (8) decreased as the thickness increased, as shown in Fig. 4S.

$$k'_1 = \frac{k_1}{P_{cal}} \text{ or } \frac{k_1}{P_{elec}} \tag{8}$$

Consequently, both the energy-modified reaction constants using calorimetric and electrical power decreased as the thickness increased. Because it is difficult to understand the effect of thickness on the sonochemical oxidation activity under limited conditions in this study, further research is required under more diverse geometric conditions.

4. Conclusions

The effects of vessel shape, vessel wall thickness, and probe position on the sonochemical oxidation activity in 20 kHz probe systems were investigated. The electrical and calorimetric power and sonochemical activity, quantified using KI dosimetry (pseudo-zero-order reaction kinetics), varied significantly as the geometric conditions changed. The trends for sonochemical activity depending on the probe position were similar in circular vessels with diameters of 5 and 10 mm and in rectangular vessel with a thickness of 5 mm. However, large differences in the sonochemical activity trends were observed for different wall thicknesses in the rectangular vessel. The highest activities were observed at probe positions of 2 and 3 cm in the rectangular vessels, whereas they were obtained at 1 cm in the circular vessels and rectangular vessels with diameters of 5 and 10 mm. Under various geometric

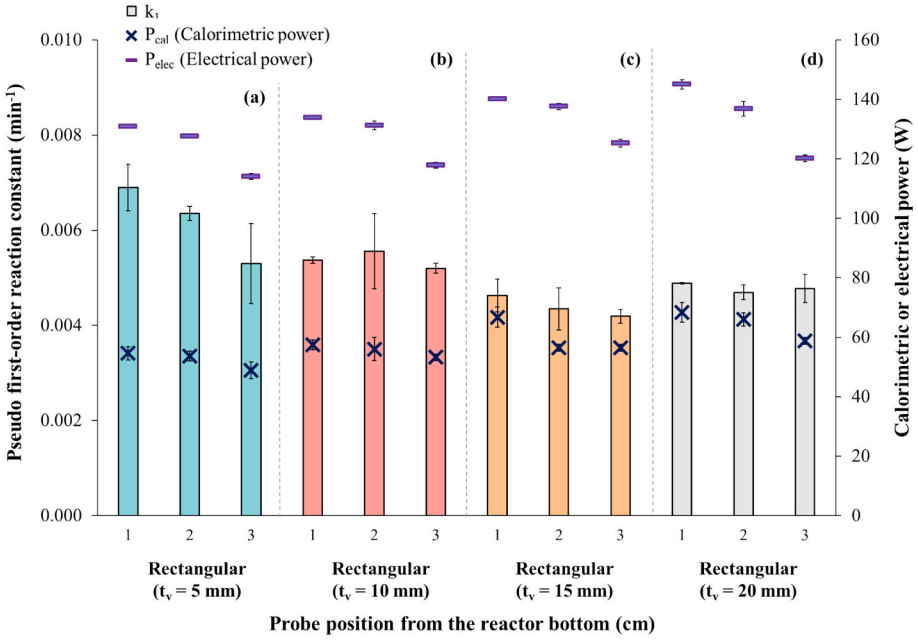

Fig. 5. Pseudo first-order reaction constants (k_1), calorimetric powers, and electrical powers for the BPA degradation under various geometric conditions (all the data points include error bars).

conditions, the SCL images demonstrated variations in the sonochemically active zones, and the hotspot positions and intensities were significantly different depending on the probe position, vessel shape, and vessel wall thickness. The SCL trends matched those of the sonochemical activity quantified using KI dosimetry. However, the trends of BPA degradation (pseudo-first-order reaction kinetics) did not match those of KI dosimetry at probe positions of 1, 2, and 3 cm for wall thicknesses of 5, 10, 15, and 20 mm in rectangular vessels. Thus, it was revealed that the geometric optimal conditions for sonochemical activity could vary significantly depending on the applied geometric conditions, and further research data should be accumulated to suggest guidelines for the appropriate use of 20 kHz probe systems.

CRediT authorship contribution statement

Chaewoon Hwang: Writing – original draft, Validation, Methodology, Investigation, Formal analysis, Data curation. **Iseul Na:** Writing – original draft, Validation, Methodology, Investigation, Formal analysis, Data curation. **Younggyu Son:** Writing – review & editing, Writing – original draft, Visualization, Validation, Supervision, Resources, Project administration, Methodology, Investigation, Formal analysis, Conceptualization.

Declaration of competing interest

The authors declare that they have no competing financial interests or personal relationships that may have influenced the work reported in this study.

Acknowledgments

This work was supported by the National Research Foundation of Korea (NRF) grant funded by the Korean Government (MSIT) [RS-2024-00350023] and the Gyeongsangbuk-do RISE (Regional Innovation System & Education) project (Specialized Industry Scale-up unit).

Appendix A. Supplementary data

Supplementary data to this article can be found online at https://doi.org/10.1016/j.ultsonch.2025.107519.

References

[1] A. Esmaeili, S. Pourranjabar Hasan Kiadeh, A. Ebrahimian Pirbazari, F. Esmaeili Khalil Saraei, A. Ebrahimian Pirbazari, A. Derakhshesh, F.-S. Tabatabai-Yazdi, CdS nanocrystallites sensitized ZnO nanosheets for visible light induced sonophotocatalytic/photocatalytic degradation of tetracycline: From experimental results to a generalized model based on machine learning methods, Chemosphere 332 (2023) 138852.
[2] G. Matafonova, V. Batoev, Review on low- and high-frequency sonolytic, sonophotolytic and sonophotochemical processes for inactivating pathogenic microorganisms in aqueous media, Water Res. 166 (2019) 115085.
[3] Y. Rao, H. Yang, D. Xue, Y. Guo, F. Qi, J. Ma, Sonolytic and sonophotolytic degradation of Carbamazepine: Kinetic and mechanisms, Ultrason. Sonochem. 32 (2016) 371–379.
[4] M. Cui, Y. Son, M. Lim, S. Na, J. Khim, Elimination of two hormones by ultrasonic and ozone combined processes, Jpn. J. Appl. Phys. 49 (2010) 07HE09.
[5] Y. Son, J. Lim, M. Cui, M. Lim, B.-Y. Kweon, J. Khim, Application of ultrasound and ozone for the removal of aqueous tannin, Jpn. J. Appl. Phys. 48 (2009) 07GH05.
[6] J. Kim, B. Park, Y. Son, J. Khim, Peat moss-derived biochar for sonocatalytic applications, Ultrason. Sonochem. 42 (2018) 26–30.
[7] A. Khataee, B. Kayan, P. Gholami, D. Kalderis, S. Akay, L. Dinpazhoh, Sonocatalytic degradation of Reactive Yellow 39 using synthesized ZrO_2 nanoparticles on biochar, Ultrason. Sonochem. 39 (2017) 540–549.
[8] K. Kang, M. Jang, M. Cui, P. Qiu, S. Na, Y. Son, J. Khim, Enhanced sonocatalytic treatment of ibuprofen by mechanical mixing and reusable magnetic core titanium dioxide, Chem. Eng. J. 264 (2015) 522–530.
[9] B. Jun, J. Choi, Y. Son, Ultrasonic activation of persulfate for the removal of BPA in 20, 28, and 300 kHz systems, Ultrason. Sonochem. 114 (2025) 107281.
[10] J. Choi, D. Lee, Y. Son, Ultrasonic activation of persulfate for removal of aqueous pollutants: cavitational versus thermal mechanisms, Curr. Opin. Chem. Eng. 48 (2025) 101136.
[11] R. James Wood, T. Sidnell, I. Ross, J. McDonough, J. Lee, M.J. Bussemaker, Ultrasonic degradation of perfluorooctane sulfonic acid (PFOS) correlated with sonochemical and sonoluminescence characterisation, Ultrason. Sonochem. 68 (2020) 105196.
[12] X. Xiong, Y. Shang, L. Bai, S. Luo, T.W. Seviour, Z. Guo, L.D.M. Ottosen, Z. Wei, Complete defluorination of perfluorooctanoic acid (PFOA) by ultrasonic pyrolysis towards zero fluoro-pollution, Water Res. 235 (2023) 119829.
[13] T. Shende, G. Andaluri, R. Suri, Power density modulated ultrasonic degradation of perfluoroalkyl substances with and without sparging Argon, Ultrason. Sonochem. 76 (2021) 105639.
[14] R.J. Wood, J. Lee, M.J. Bussemaker, A parametric review of sonochemistry: Control and augmentation of sonochemical activity in aqueous solutions, Ultrason. Sonochem. 38 (2017) 351–370.
[15] Y. Son, Advanced Oxidation Processes using Ultrasound Technology for Water and Wastewater Treatment, in: M. Ashokkumar (Ed.), Handbook of Ultrasonics and Sonochemistry, Springer Singapore, Singapore, 2016, pp. 1–22.
[16] I. Na, Y. Son, Sonochemical oxidation activity in 20-kHz probe-type sonicator systems: the effects of probe positions and vessel sizes, Ultrason. Sonochem. 108 (2024) 106959.
[17] Y. Son, J. Choi, Effects of gas saturation and sparging on sonochemical oxidation activity in open and closed systems, part II: NO_2^-/NO_3^- generation and a brief critical review, Ultrason. Sonochem. 92 (2023) 106250.
[18] S. Lee, Y. Son, Effects of gas saturation and sparging on sonochemical oxidation activity under different liquid level and volume conditions in 300-kHz sonoreactors: Zeroth- and first-order reaction comparison using KI dosimetry and BPA degradation, Ultrason. Sonochem. 98 (2023) 106521.
[19] D. Lee, J. Kang, Y. Son, Effect of violent mixing on sonochemical oxidation activity under various geometric conditions in 28-kHz sonoreactor, Ultrason. Sonochem. 101 (2023) 106659.
[20] J. Choi, Y. Son, Effect of dissolved gases on sonochemical oxidation in a 20 kHz probe system: Continuous monitoring of dissolved oxygen concentration and sonochemical oxidation activity, Ultrason. Sonochem. 97 (2023) 106452.
[21] Y. Son, J. Seo, Effects of gas saturation and sparging on sonochemical oxidation activity in open and closed systems, Part I: H_2O_2 generation, Ultrason. Sonochem. 90 (2022) 106214.
[22] J. Choi, H. Lee, Y. Son, Effects of gas sparging and mechanical mixing on sonochemical oxidation activity, Ultrason. Sonochem. 70 (2021) 105334.
[23] Y. Son, Y. No, J. Kim, Geometric and operational optimization of 20-kHz probe-type sonoreactor for enhancing sonochemical activity, Ultrason. Sonochem. 65 (2020) 105065.
[24] J. Choi, J. Khim, B. Neppolian, Y. Son, Enhancement of sonochemical oxidation reactions using air sparging in a 36 kHz sonoreactor, Ultrason. Sonochem. 51 (2019) 412–418.
[25] Y. Son, Simple design strategy for bath-type high-frequency sonoreactors, Chem. Eng. J. 328 (2017) 654–664.
[26] Y. Son, M. Lim, M. Ashokkumar, J. Khim, Geometric optimization of sonoreactors for the enhancement of sonochemical activity, J. Phys. Chem. C 115 (2011) 4096–4103.
[27] T. Khuyen Viet Bao, A. Yoshiyuki, K. Shinobu, Influence of Liquid Height on Mechanical and Chemical Effects in 20 kHz Sonication, Jpn. J. Appl. Phys. 52 (2013) 07HE07.
[28] Y. Asakura, T. Nishida, T. Matsuoka, S. Koda, Effects of ultrasonic frequency and liquid height on sonochemical efficiency of large-scale sonochemical reactors, Ultrason. Sonochem. 15 (2008) 244–250.
[29] K. Yoshihiro, K. Shinobu, N. Hiroyasu, Effects of sample volume and frequency on ultrasonic power in solutions on sonication, Jpn. J. Appl. Phys. 37 (1998) 2992.
[30] D. Kobayashi, K. Sano, Y. Takeuchi, K. Terasaka, Effect of irradiation distance on degradation of phenol using indirect ultrasonic irradiation method, Ultrason. Sonochem. 18 (2011) 1205–1210.
[31] D. Kobayashi, H. Matsumoto, C. Kuroda, Effect of reactor's positions on polymerization and degradation in an ultrasonic field, Ultrason. Sonochem. 15 (2008) 251–256.
[32] P.R. Gogate, V.S. Sutkar, A.B. Pandit, Sonochemical reactors: Important design and scale up considerations with a special emphasis on heterogeneous systems, Chem. Eng. J. 166 (2011) 1066–1082.
[33] I. Na, T. Kim, P. Qiu, Y. Son, Machine learning model to predict rate constants for sonochemical degradation of organic pollutants, Ultrason. Sonochem. 110 (2024) 107032.
[34] A. Konya, P. Nematzadeh, Recent applications of AI to environmental disciplines: a review, Sci. Total Environ. 906 (2024) 167705.
[35] S.-Z. Zhang, S. Chen, H. Jiang, A new tool to predict the advanced oxidation process efficiency: using machine learning methods to predict the degradation of organic pollutants with Fe-carbon catalyst as a sample, Chem. Eng. Sci. 280 (2023) 119069.
[36] Y. No, Y. Son, Effects of probe position of 20 kHz sonicator on sonochemical oxidation activity, Jpn. J. Appl. Phys. 58 (2019) SGGD02.
[37] J. Choi, Y. Son, Quantification of sonochemical and sonophysical effects in a 20 kHz probe-type sonoreactor: Enhancing sonophysical effects in heterogeneous systems with milli-sized particles, Ultrason. Sonochem. 82 (2022) 105888.
[38] J.K. Chu, T.J. Tiong, S. Chong, U.A. Asli, Y.H. Yap, Multi-frequency sonoreactor characterisation in the frequency domain using a semi-empirical bubbly liquid model, Ultrason. Sonochem. 80 (2021) 105818.
[39] T.J. Tiong, D.K.L. Liew, R.C. Gondipon, R.W. Wong, Y.L. Loo, M.S.T. Lok, S. Manickam, Identification of active sonochemical zones in a triple frequency ultrasonic reactor via physical and chemical characterization techniques, Ultrason. Sonochem. 35 (2017) 569–576.

[40] Y. Asakura, S. Fukutomi, K. Yasuda, S. Koda, Optimization of sonochemical reactors by measuring impedance of transducer and sound pressure in solution, J. Chem. Eng. Jpn 43 (2010) 1008–1013.
[41] K. Yasuda, T. Yamazaki, Y. Asakura, Dependence of reaction on vessel position, diameter, and liquid height in the sonochemical reactor with indirect irradiation, Jpn. J. Appl. Phys. 63 (2024) 04SP12.
[42] J.-M. Löning, C. Horst, U. Hoffmann, Investigations on the energy conversion in sonochemical processes, Ultrason. Sonochem. 9 (2002) 169–179.
[43] M. Lim, M. Ashokkumar, Y. Son, The effects of liquid height/volume, initial concentration of reactant and acoustic power on sonochemical oxidation, Ultrason. Sonochem. 21 (2014) 1988–1993.
[44] K. Thangavadivel, K. Okitsu, G. Owens, P.J. Lesniewski, R. Nishimura, Influence of sonochemical reactor diameter and liquid height on methyl orange degradation under 200kHz indirect sonication, J. Environ. Chem. Eng. 1 (2013) 275–280.
[45] Y. Son, M. Lim, J. Song, J. Khim, Liquid height effect on sonochemical reactions in a 35 kHz sonoreactor, Jpn. J. Appl. Phys. 48 (2009) 07GM16.
[46] P. Dou, Y. Jia, P. Zheng, T. Wu, M. Yu, T. Reddyhoff, Z. Peng, Review of ultrasonic-based technology for oil film thickness measurement in lubrication, Tri. Int. 165 (2022) 107290.
[47] C.-W. Chung, J.S. Popovics, L.J. Struble, Using ultrasonic wave reflection to measure solution properties, Ultrason. Sonochem. 17 (2010) 266–272.
[48] J. Klíma, A. Frias-Ferrer, J. González-García, J. Ludvík, V. Sáez, J. Iniesta, Optimisation of 20kHz sonoreactor geometry on the basis of numerical simulation of local ultrasonic intensity and qualitative comparison with experimental results, Ultrason. Sonochem. 14 (2007) 19–28.
[49] S. Fukunaga, S. Higashi, T. Horie, H. Sugiyama, A. Kanda, T.-Y. Hsu, K.-L. Tung, K. Taniya, S. Nishiyama, N. Ohmura, Effect of geometrical configuration of reactor on a ZrP nano-dispersion process using ultrasonic irradiation, Ultrason. Sonochem. 52 (2019) 157–163.
[50] Y. Son, M. Lim, J. Khim, L.-H. Kim, M. Ashokkumar, Comparison of calorimetric energy and cavitation energy for the removal of bisphenol-A: the effects of frequency and liquid height, Chem. Eng. J. 183 (2012) 39–45.
[51] M. Toma, S. Fukutomi, Y. Asakura, S. Koda, A calorimetric study of energy conversion efficiency of a sonochemical reactor at 500 kHz for organic solvents, Ultrason. Sonochem. 18 (2011) 197–208.
[52] B. Yang, M. Ye, S. Ren, L. Liu, Optimizing cavitation performance in bath-type sonoreactor by numerical simulation combining the Keller-Miksis equation and nonlinear Helmholtz equation, Chem. Eng. J. 510 (2025) 161696.
[53] K. Yasui, T. Kozuka, T. Tuziuti, A. Towata, Y. Iida, J. King, P. Macey, FEM calculation of an acoustic field in a sonochemical reactor, Ultrason. Sonochem. 14 (2007) 605–614.
[54] D. Lee, I. Na, Y. Son, Effect of liquid recirculation flow on sonochemical oxidation activity in a 28 kHz sonoreactor, Chemosphere 286 (2022) 131780.